MATERIALS SCIENCE

A predictive framework for the design and fabrication of icephobic polymers

Kevin Golovin[1,2]* and Anish Tuteja[1,2,3,4]†

Ice accretion remains a costly, hazardous concern worldwide. Icephobic coatings reduce the adhesion between ice and a surface. However, only a handful of the icephobic systems reported to date reduce the ice adhesion sufficiently for the facile and passive removal of ice, such as under its own weight or by mild winds. Most of these icephobic surfaces have relied on sacrificial lubricants, which may be depleted over time, drastically raising the ice adhesion. In contrast, surfaces that use interfacial slippage to lower their adhesion to ice can remain icephobic indefinitely. However, the mechanism of interfacial slippage, as it relates to ice adhesion, is largely unexplored. We investigate how interfacial slippage reduces the ice adhesion of polymeric materials. We propose a new, universally applicable framework that may be used to predict the reduction in the adhesion of ice to surfaces exhibiting interfacial slippage. This framework allows one to rationally engender icephobicity in essentially any polymeric system, including common thermoplastics. Hence, we present several new, extremely icephobic systems fabricated from a wide range of materials, including everyday engineering plastics and sustainable, natural oils.

INTRODUCTION

The removal of accreted ice remains a costly, hazardous concern, both residentially and industrially across the globe (*1*, *2*). Coatings that significantly reduce the adhesion between ice and a given surface can be called icephobic (*3*). However, very few coatings have been fabricated that facilitate the complete removal of ice without the input of additional energy, that is, surfaces where ice may be removed by its own weight (*4*–*11*). Typically, these extremely icephobic surfaces have relied on sacrificial lubricants, where the icephobic properties may diminish as the lubricant becomes depleted. There are currently no methods for predicting the resultant ice adhesion once the lubricant has been removed. This inability to predict the ice adhesion is not limited to initially lubricated surfaces. Although it would be highly desirable, there is not a single reported method for modifying the icephobicity of a given surface in a predictable manner.

Materials like glass, steel, and aluminum display ice adhesion strengths of $\tau_{ice} > 1000$ kPa (*7*, *12*). The ice adhesion strength of polymeric systems typically ranges 150 kPa $\leq \tau_{ice} \leq$ 500 kPa (*12*, *13*). However, for ice to be removed by wind shear or solely under its own weight, significantly lower τ_{ice} values are necessary. For example, ice accumulation notoriously lowers the efficiency of wind turbines during the winter months (*14*). A typical offshore wind turbine blade is 85 m long and rotates at a minimum speed of 10 rpm (*15*). At the blade tip, the centripetal force experienced by a square meter slab of ice that is 1 cm thick is around 12 kN. For this ice to detach, $\tau_{ice} \leq 12$ kPa is necessary. This order-of-magnitude disparity highlights the inherent difficulty in fabricating practically useful icephobic surfaces.

Recently, we showed that low-modulus (or low cross-link density, ρ^{CL}) elastomers are intrinsically icephobic (*7*). When ice adhered to a low-ρ^{CL} elastomer experiences a shear stress, the ice-elastomer interface can cavitate, causing the ice to detach at low applied loads (*16*). Ice adhesion strengths as low as $\tau_{ice} \approx 10$ kPa were reported for dry, low-modulus elastomers. However, these extremely soft surfaces are not mechanically robust. Therefore, low ρ^{CL} alone offers limited improvement, in terms of durability toward repeated icing/deicing, over lubricated systems that initially display equally low ice adhesion strengths (*4*, *9*, *10*). Fortunately, engendering slip at the ice interface can further reduce the adhesion of ice to elastomers.

The no-slip condition is a ubiquitous boundary condition found in the areas of fluid mechanics (*17*), polymer rheology (*18*), and contact mechanics (*19*). Here, the no-slip condition refers to a solid coating remaining rigidly adhered to ice during the application of an external load (but before fracture). In contrast, if the interface is sufficiently mobile, slip between the ice and the coating can occur in a process referred to as interfacial slippage (*20*). In our previous work, we showed that elastomers exhibiting interfacial slippage displayed a significantly reduced adhesion to ice (*7*). Interfacial slippage was achieved for some of the fabricated coatings by filling the different elastomers with various oils. Although we observed interfacial slippage to be most effective for low-ρ^{CL} elastomers, the extent to which an oil caused interfacial slippage remained largely unexplored. Here, we develop a framework that predicts the reduction in the ice adhesion of surfaces using interfacial slippage, as well as τ_{ice} for lubricated surfaces that have lost their lubricating oil layer. This framework allows one to quantitatively predict the reduction in τ_{ice} and, therefore, enables the design of extremely icephobic surfaces fabricated from essentially any polymeric system, including non–cross-linked thermoplastics, knowing only the properties of the initial polymer and oil. Although some work has previously been done on rendering cross-linked networks icephobic (*6*, *7*, *9*–*11*, *13*, *21*, *22*), there are no reported methods for fabricating icephobic systems from common engineering plastics.

Framework

The purpose of this work is to understand how the ice adhesion of polymers changes when they are plasticized. We will refer to the miscible liquid component within the polymer interchangeably as an oil or a plasticizer, although we recognize that only a subset of polymers may be plasticized with oils and that not all plasticizers are oily (*23*). To predict the reduction in ice adhesion of any plasticized polymer, we will show that only two properties need be known: τ_{ice}^{no-oil}, the ice adhesion strength of the unfilled (dry) polymer, and ϕ_{oil}^{max}, the maximum plasticizer content

[1]Department of Materials Science and Engineering, University of Michigan, Ann Arbor, MI 48109, USA. [2]Biointerfaces Institute, University of Michigan, Ann Arbor, MI 48109, USA. [3]Department of Chemical Engineering, University of Michigan, Ann Arbor, MI 48109, USA. [4]Department of Macromolecular Science and Engineering, University of Michigan, Ann Arbor, MI 48109, USA.
*Present address: HygraTek LLC, 1600 Huron Parkway, Building 520, Suite 2393, Ann Arbor, MI 48109, USA.
†Corresponding author. Email: atuteja@umich.edu

of the polymer before complete phase separation occurs (that is, the miscibility limit of the plasticizer in the polymer).

On the basis of Chernyak and Leonov's framework for the friction of rubber (*19*), we previously showed that when interfacial slippage was enabled

$$\frac{\tau_{ice}^{oil}}{\tau_{ice}^{no-oil}} \propto \frac{\rho_{oil}^{CL}}{\rho_{no-oil}^{CL}} \quad (1)$$

where we use "oil" and "no-oil" to denote either the ice adhesion strength, or the cross-link density, of the swollen (with oil) and dry (without oil) polymer, respectively. The reduction in ice adhesion of an oil-filled network was shown to be directly proportional to the reduction in the cross-link density of the network. It is well known that filling a polymer with a liquid lowers its effective cross-link density (*24*). To predict the reduction in ice adhesion caused by filling a polymer with oil, a relation between ρ^{CL} and bulk oil content, ϕ_{oil}, is needed. Below, we derive such a relation.

If interfacial slippage occurs, then the reduction in ice adhesion was shown to strongly depend on the ρ^{CL}. For example, a 24-fold reduction in τ_{ice} was observed for a soft polyurethane rubber, and essentially, no change in τ_{ice} was observed for rigid plastics like polystyrene (PS) (*7*). However, modification of the base material was necessary to achieve identical modulus values for comparing surfaces that did, and did not, exhibit interfacial slippage. Here, we discuss the more general case, where both the cross-link density and interfacial slippage are allowed to vary for each polymer/oil combination. Essentially, we answer the question: For surfaces exhibiting interfacial slippage, how does τ_{ice} depend on ϕ_{oil}?

In our proposed framework for interfacial slippage, we assume that the ice adhesion of pure oil is negligible. Because liquids may be defined by their inability to support shear, this is a reasonable assumption (*25*). Highly lubricated systems have approached this idealization, initially displaying τ_{ice} = 1.7 kPa (*10*), τ_{ice} = 1.4 kPa (*9*), and τ_{ice} = 0.15 kPa (*7*). At the ice-polymer interface, we let ϕ_s be the fraction of solid polymer in contact with ice. The remaining $1 - \phi_s$ of the surface is composed of oil, and a lubricated surface may be defined such that $\phi_s = 0$. We propose that the ice adhesion strength of an oil-filled polymer is given by

$$\tau_{ice}^{oil} = \tau_{ice}^{no-oil} \frac{\rho_{oil}^{CL}}{\rho_{no-oil}^{CL}} \phi_s \quad (2)$$

Equation 2 combines the reduction in cross-link density through the addition of oil, or relation (1), with the reduction in adhesion sites at the surface of the filled polymer. The linear scaling with ϕ_s has the advantage of bounding the ice adhesion of the oil-filled polymer between $\tau_{ice} = \tau_{ice}^{no-oil}$, when $\phi_{oil} = 0$, and $\tau_{ice} = 0$ when the surface is fully lubricated. To measure ϕ_s, we use the theory of hemi-wicking first proposed by Bico *et al.* for rough, partially wetted surfaces (*26*).

RESULTS

Theory

The Flory-Rehner relation has been successfully used since 1943 to describe how cross-linked networks swell in the presence of liquids (*24*). It is often written as

$$\rho^{CL} = \frac{\ln(1 - \nu_2) + \nu_2 + \chi\nu_2^2}{V_1(\nu_2^{1/3} - 0.5\nu_2)} \quad (3)$$

where ν_2 is the volume fraction of polymer in a swollen gel and χ is the Flory-Huggins interaction parameter between the polymer and the probe solvent, with molecular volume V_1. Flory and Rehner (*24*) originally derived this equation for natural rubber vulcanates, which are often filled with carbon black. Twenty years later, Kraus (*27*) extended the Flory-Rehner equation to account for these rigid fillers within the elastic network that would not swell in the presence of a solvent. If S is the apparent swell ratio of a filled rubber, and S_o is the swell ratio of the unfilled rubber, Kraus proposed that $S = (S_o - \phi)/(1 - \phi)$, where ϕ is the volume fraction of filler. This relation suggests that only the volume of rubber, $(1 - \phi)$, can be swollen by the solvent. For our purposes, this can be rewritten as

$$\nu_2^{oil} = \nu_2(1 - \phi)/(1 - \nu_2\phi) \quad (4)$$

where ν_2^{oil} is the apparent volume fraction of polymer (that had been filled with oil) in a swollen gel and ν_2 is the volume fraction of polymer (that was initially unfilled) in the gel. Recall that $\nu_2 = S_o^{-1}$, and similarly, $\nu_2^{oil} = S^{-1}$. For particulate fillers, Kraus showed that the filler-rubber bond strength limited the final swell ratio by some swelling deficiency, $\Delta\nu$. Here, the filler is an oil, which may be displaced by the solvent upon swelling, making polymers prefilled with oil an idealized case where $\Delta\nu = 0$. When we swelled seven different oil-filled networks (Materials and Methods and Fig. 1A), a good agreement was observed between our experimental swell ratios and Eq. 4. We normalize ϕ_{oil} by its maximum value, ϕ_{oil}^{max}, for readability purposes only in Fig. 1A. Recalling relation (1) from above, the reduction in ρ^{CL} of a cross-linked network, due to swelling by an oil, is proportional to the reduction in ice adhesion. The cross-link density of an oil-filled polymer can be found by substituting Eq. 4 into the Flory-Rehner relation. Dividing the relation for the filled cross-link density by its unfilled counterpart yields

$$\frac{\rho_{oil}^{CL}}{\rho_{no-oil}^{CL}} = \frac{\left(\ln\left(\frac{\nu_2(1-\phi)}{(1-\nu_2\phi)}\right) + \chi\left(\frac{\nu_2(1-\phi)}{(1-\nu_2\phi)}\right)^2 + \frac{\nu_2(1-\phi)}{(1-\nu_2\phi)}\right)\left(\nu_2^{1/3} - \frac{\nu_2}{2}\right)}{(\ln(1-\nu_2) + \nu_2 + \chi\nu_2^2)\left(\left(\frac{\nu_2(1-\phi)}{(1-\nu_2\phi)}\right)^{1/3} - \frac{\nu_2(1-\phi)}{2(1-\nu_2\phi)}\right)} \quad (5)$$

For large swell ratios (small values of ν_2), Eq. 5 reduces to (see the Supplementary Materials)

$$\frac{\rho_{oil}^{CL}}{\rho_{no-oil}^{CL}} = (1 - \phi)^{5/3} \quad (6)$$

An appropriate choice of solvent can always be made such that ν_2 is sufficiently small (highly swollen state), meaning that Eq. 6 is not an approximation. Equation 6 makes intuitive sense because ρ^{CL} is a property of the cross-linked network and does not depend on the solvent used to measure it. Accordingly, all the solvent-specific properties used to measure ρ^{CL} (namely, ν_2, V_1, and χ) are absent in Eq. 6. The degree by which ρ^{CL} is reduced when filled with oil solely depends on ϕ_{oil}. Note that Flory and Rehner also observed an exponential dependence of $^5/_3$ between ρ^{CL} and ν_2 when they neglected the heat of dilution and assumed that ν_2 was small in their original work (see the Supplementary Materials) (*24*). In Fig. 1B, we show an excellent agreement between Eq. 6 and three different cross-linked networks filled with seven different oils (Materials and Methods). Thus, Eq. 6 describes

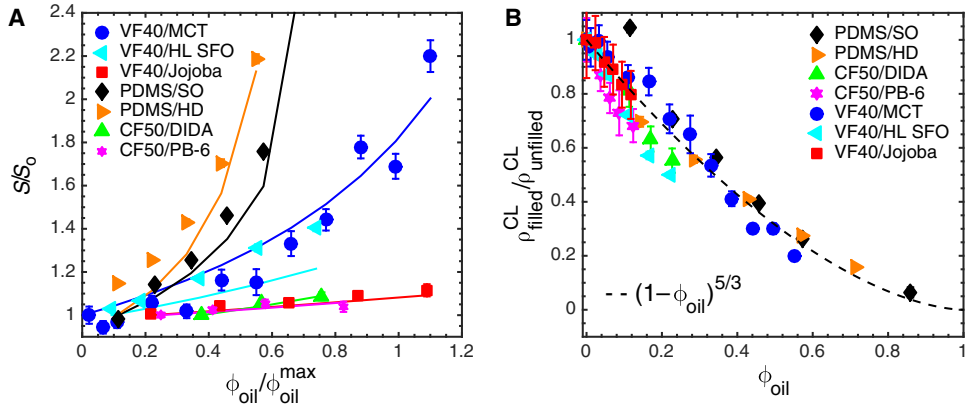

Fig. 1. The cross-link density reduction of oil-filled networks. (**A**) Ratio of the apparent swell ratio to the unfilled swell ratio (no oil) for seven different polymer/oil combinations, versus the oil content. The oil content has been normalized by the maximum oil solubility within the cross-linked network for readability purposes only. The solid lines represent Eq. 4. (**B**) Cross-link density reduction for the same seven polymer/oil combinations.

how a certain amount of oil reduces the cross-link density of a polymer, up to ϕ_{oil}^{max}.

In a binary mixture, the lower–surface energy species preferentially migrates to the interface until the gain in surface energy equilibrates with the loss in translational entropy in the bulk (*25*, *28*). To measure the amount of each component in the binary mixture on the surface, we used the theory of hemi-wicking (*26*). According to the theory of hemi-wicking, the apparent contact angle (θ*) of a liquid on a film composed of the same liquid is θ* = 0°, that is, the liquid perfectly wets itself. Contrastingly, the equilibrium contact angle of the liquid on a polymer is given by some (usually) nonzero value, θ. Hence, the apparent contact angle of an oil on an oil-filled polymer with some fraction of the same oil on its surface may be found using (*25*, *26*)

$$\cos\theta^* = (1 - \phi_s)\cos 0^\circ + \phi_s \cos\theta \quad (7)$$

where we recall that ϕ_s is the solid fraction of polymer on the surface. The embedded oil within the polymer can be used as a probe liquid when measuring contact angles to find the fraction of oil on the surface, $(1 - \phi_s)$. If the polymer is completely covered by a film of oil, then θ* = 0°. In Fig. 2A, we show the measured surface fraction of a polyurethane rubber, filled with various amounts of six different oils (Materials and Methods).

Because the solubility of a plasticizer within a polymer depends on its chemical composition (*29*), full surface coverage ($\phi_s = 0$) was reached at different ϕ_{oil} values for different oils. For example, oil derived from the seeds of the *Simmondsia chinensis* plant (jojoba oil) fully covered the surface of a polyurethane rubber around $\phi_{oil} \approx 0.1$. Fractionated coconut oil (also called medium-chain triglyceride or MCT oil) did not reach full surface coverage until $\phi_{oil} \approx 0.7$. By swelling pieces of dry polymer in each oil, ϕ_{oil}^{max} can be measured once a constant mass has been achieved (Materials and Methods and table S1) (*30*). Normalizing the fraction of oil within the rubber by ϕ_{oil}^{max} collapsed all our ϕ_s measurements (Fig. 2B). The slope of the best-fit line was $\alpha = 0.7114$, and the solid fraction at $\phi_{oil} = 0$ was set to $\phi_s = 1.0$. This yielded

$$\phi_s = 1 - \alpha\phi_{oil}/\phi_{oil}^{max} \quad (8)$$

This linear relationship is a quantitative relation between the amount of oil within the bulk of a plasticized polymer and the amount of oil on the surface of the polymer. As expected on the basis of Eq. 8, we observed $\phi_s \neq 0$ when $\phi_{oil} = \phi_{oil}^{max}$, meaning that the formation of a free oil film on the surface of the polymer required $\phi_{oil} > \phi_{oil}^{max}$. We always found that additional oil was necessary before θ* = 0°, and consequently, $\tau_{ice} \approx 0$.

Substituting Eqs. 6 and 8 into Eq. 2 yielded Eq. 9

$$\frac{\tau_{ice}^{oil}}{\tau_{ice}^{no-oil}} = (1 - \phi_{oil})^{5/3}(1 - \alpha\phi_{oil}/\phi_{oil}^{max}) \quad (9)$$

Here, the left-hand side indicates the reduction in the ice adhesion of the polymer through the addition of oil. The right-hand side is composed of two terms. The first term gives the reduction in the ice adhesion strength due to a decrease in the cross-link density of the network, and the second term represents the amount of solid polymer on the surface capable of forming an adhesive bond with ice. Again, we assume that no adhesive bond forms on the fraction of oil partially covering the surface of the polymer, $(1 - \phi_s)$. We now discuss the validity of Eq. 9 for a wide range of polymeric systems.

Icephobic cross-linked networks (thermosets)

For highly compatible plasticizer/polymer combinations, the $(1 - \phi_{oil})^{5/3}$ term dominates Eq. 9. Hence, even relatively large amounts of oil within the network will not drastically reduce the ice adhesion strength. Moreover, when the surface energy of the polymer is lower than the surface tension of the plasticizer, the decrease in ice adhesion will solely depend on the reduction in cross-link density (that is, $\phi_s = 1.0$). In this case, Eq. 9 would reduce to

$$\frac{\tau_{ice}^{oil}}{\tau_{ice}^{no-oil}} = (1 - \phi_{oil})^{5/3} \quad (10)$$

MCT oil displayed high ($\phi_{oil}^{max} \approx 0.5$) miscibility in the polyurethane rubber VytaFlex 40 (VF40). As Fig. 3A shows, Eq. 9 was a very good approximation for the ice adhesion strength of VF40 filled with MCT oil, especially for $\phi_{oil} \geq 0.2$. Moreover, although MCT oil was highly

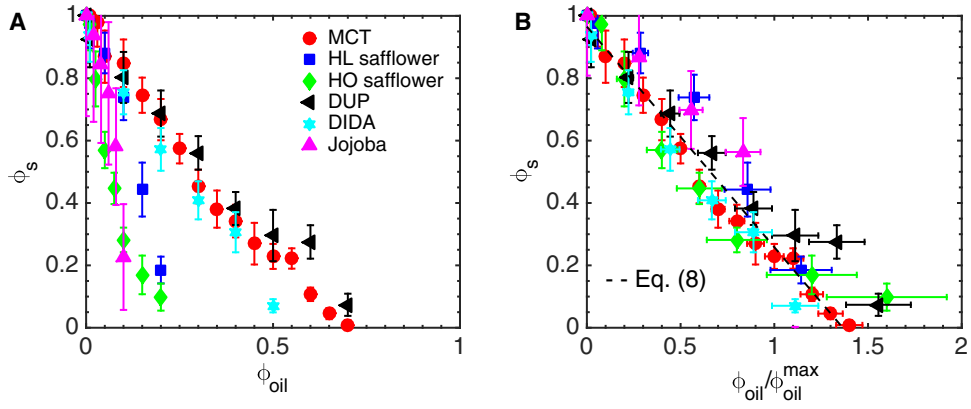

Fig. 2. The surface fraction of oil-filled networks. (**A**) Solid fraction of an oil-filled, cross-linked network versus the oil content within the network. (**B**) These data collapse when the oil content is normalized by its maximum solubility within the cross-linked material. HO, high-oleic; DUP, diundecyl phthalate.

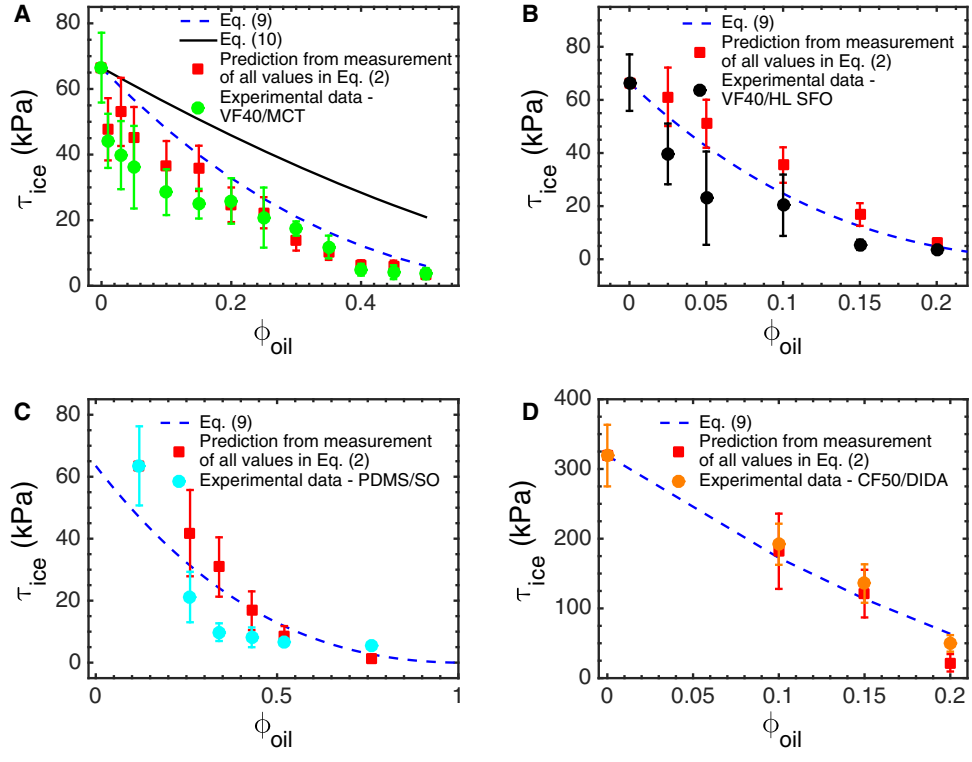

Fig. 3. Icephobic cross-linked networks. Ice adhesion strength versus oil content for four different polymer/oil combinations. (**A**) VF40 filled with MCT oil. (**B**) VF40 filled with HL SFO. (**C**) PDMS filled with silicone oil. (**D**) CF50 filled with DIDA. For all these surfaces, the inputs to Eq. 2 can be found by experimentally measuring ρ^{CL} and ϕ_s. The measured predictions using Eq. 2 are shown as red squares in (A) to (D).

miscible with the rubber, Eq. 10 did not fully capture the observed reduction in τ_{ice}. The reduced ice adhesion strength depended on both the cross-link density decrease and the presence of oil on the surface. To contrast this, we also filled a fluorinated polyurethane (FPU) with high-linoleic safflower oil (HL SFO) (Materials and Methods). For this system, the surface energy of the fluorinated network was lower than the surface tension of the plasticizer. Hence, the observed ice adhesion strength followed Eq. 10 (as discussed below).

In Fig. 3, we present three data sets for four different cross-linked networks. First, we predicted the reduction in ice adhesion through Eq. 9, using the ice adhesion strength of the unfilled elastomer (τ_{ice}^{no-oil}) and the value of ϕ_{oil}^{max} (see Table 1). Second, we measured the actual surface fraction, the cross-link density of the unfilled and oil-filled rubbers, and τ_{ice}^{no-oil} and substituted these values into Eq. 2 (red squares in Fig. 3). Third, we experimentally measured the ice adhesion strength of the oil-filled elastomers (circles, Fig. 3). The discrepancy between the experimental data (circles) and the prediction using Eq. 2 (red squares) indicated how appropriate our framework was for predicting the ice adhesion strength of each system. The discrepancy between Eq. 9 and the values found using Eq. 2 indicated how closely our

Table 1. The optimal composition and resultant ice adhesion strength for 10 different icephobic polymer/plasticizer combinations fabricated in this work. The amount of oil in each system was optimized for both low ice adhesion and good mechanical durability. For a complete list of surfaces, see table S2. PVC, polyvinyl chloride. *The ϕ_{oil}^{max} values for plasticized PVC and PS were found using a best fit to Eq. 9 and do not represent values obtained by swell tests.

Base	Oil (ϕ_{oil}^{max})	ϕ_{oil}	τ_{ice} (kPa)
PDMS	Silicone (1.0)	0.5	6.5 ± 1.0
VF40	MCT (0.51)	0.4	4.9 ± 1.8
VF40	HL SFO (0.3)	0.15	4.3 ± 1.0
VF40	Eucalyptus (0.8)	0.5	11 ± 4
CF50	DIDA (0.25)	0.2	50 ± 12
CF50VF20	MCT (0.36)	0.35	9.0 ± 3.0
PVC	MCT (0.9)*	0.85	5.2 ± 2.7
PVC	DIDA (0.86)*	0.75	16 ± 5
PS	DIDA (0.16)*	0.2	27 ± 6
PS	MCT (0.16)*	0.2	24 ± 8

approximations for the cross-link density and surface fraction were to their measured values. A good agreement was observed between the framework (Eq. 2), the simplified framework (Eq. 9), and the experimental data.

Equation 9 also predicted the reduction in ice adhesion strength for polymer/oil combinations with poor compatibility. In contrast to the highly miscible MCT oil, HL SFO showed limited solubility within the VF40 rubber (a complete oil film formed around $\phi_{oil} \approx 0.2$). However, a good agreement was still observed for the VF40/HL SFO system (Fig. 3B). We found Eq. 9 universally applied to many different polymer/oil combinations, including polydimethylsiloxane (PDMS) filled with silicone oil (Fig. 3C) and the polyurethane rubber Clear Flex 50 (CF50) swollen with diisodecyl adipate (DIDA; Fig. 3D). Note that, in the case of CF50, the ice adhesion strength of the dry polymer is quite high ($\tau_{ice} > 300$ kPa). Therefore, icephobic polymers may be fabricated from highly non-icephobic base materials through the addition of a miscible oil, and the effect of the addition of oil can be described by Eq. 9.

Icephobic linear polymers (thermoplastics)

The five systems discussed above were all based on chemically cross-linked networks (thermosets) filled with various oils. We now show that the applicability of Eq. 9 also extended to linear polymers (thermoplastics). Linear polymers owe their mechanical properties to crystallinity and/or the physical entanglement of chains; there are no chemical cross-links (*31*). The mechanical properties of linear polymers can be highly affected by plasticizing agents (*23*). We studied the ice adhesion of two common, linear polymers, PVC and PS, plasticized with MCT oil or DIDA. Besides the lack of chemical cross-links, the key difference between the elastomeric rubbers studied above and the linear polymers studied here was ϕ_{oil}^{max}. Both MCT oil and DIDA dissolve PS and PVC, meaning that $\phi_{oil}^{max} \approx 1.0$ for these two plasticizing agents.

When we evaluated the ice adhesion strength of PVC, plasticized with either MCT oil or DIDA, a good agreement was still observed with Eq. 9 (Fig. 4A). Even under the assumption that there was no plasticizer present on the PVC surface, making Eq. 10 valid, a decent agreement was still found between our framework and the measured ice adhesion strengths (although Eq. 9 was still a better predictor, because both MCT oil and DIDA exhibit lower surface tension than the surface energy of PVC). Allowing ϕ_{oil}^{max} to vary as a free parameter, the best fit to Eq. 9 for PVC was $\phi_{oil}^{max} \approx 0.9$ for both plasticizers. Accordingly, PVC plasticized with 85 weight % (wt %) MCT oil displayed an ice adhesion strength of $\tau_{ice} = 5.2 \pm 2.7$ kPa, although there was no observable free oil layer on the surface of the coating, and the ice adhesion strength did not increase over 10 icing/deicing cycles (fig. S1). The PVC/MCT system is particularly promising because, when $0.6 \leq \phi_{oil} \leq 0.9$, the coating is predominantly composed of nontoxic, biorenewable materials, the material is >99% transparent (Fig. 4B), the mechanical properties are highly tunable, and the observed ice adhesion strength was always $\tau_{ice} \leq 25$ kPa.

Dissimilar to PVC, PS's mechanical properties were greatly altered by small amounts of plasticizing agents. A mixture of PS + 25 wt % MCT oil, or DIDA, was a viscous liquid at room temperature ($\tau_{ice} \approx 0$). In contrast, the ice adhesion strength for PVC + 50 wt % MCT oil was $\tau_{ice} > 100$ kPa, because the surface was a semirigid plastic. Despite this difference, Eq. 9 still accurately predicted the reduction in the ice adhesion strength of plasticized PS (Fig. 4C), along with other linear polymers such as ethyl cellulose and chlorinated polyisobutylene (Fig. 4D).

By normalizing the plasticizer content by ϕ_{oil}^{max}, a few trends became apparent. First, systems with limited oil solubility followed nearly linear reductions in ice adhesion with increasing oil content. At low values of ϕ_{oil}, relative to ϕ_{oil}^{max}, the cross-link density term in Eq. 9 is insignificant, and the reduction in τ_{ice} will be dominated by the linear reduction in ϕ_s with increasing ϕ_{oil}. This was observed for the CF50/DIDA, PS/MCT, PS/DIDA, and VF40/jojoba oil combinations. All these systems displayed $\phi_{oil}^{max} \leq 0.2$. Second, because the reduction in τ_{ice} is highly predictable using Eq. 9, equally icephobic systems can be designed such that ϕ_{oil} is intentionally very small or very large. A small ϕ_{oil} would require minimal operational changes from the production of the base material. A coating with a large ϕ_{oil} could be environmentally friendly and easily processed, because most of the icephobic material could be fabricated from low-viscosity, natural oils.

DISCUSSION

Designing icephobic surfaces

Designing icephobic polymers requires the knowledge of only the inherent ice adhesion strength of the dry polymer (τ_{ice}^{no-oil}) and the maximum oil content that the polymer can uptake (ϕ_{oil}^{max}). In Fig. 5A, we construct a phase diagram for icephobic polymers. An upper bound to the ice adhesion strength reduction occurs when no plasticizer is present on the surface of the polymer. In this case, Eq. 10 describes the minimal possible reduction in τ_{ice} for the plasticized polymer, arising solely from the reduction in the modulus. The red region of our phase diagram (Fig. 5A) encompasses ice adhesion strengths higher than our framework allows. Because the oil can only exist within the bulk of the polymer, or on its surface, ice adhesion strengths within this regime should never be observed, unless the adhesion of ice to the oil is nonzero. In our previous work (*7*), we fabricated one such exceptional system: PS filled with liquid, low–molecular weight ($M_w = 200$ g/mol) PS. Upon evaluation of a pure film of this liquid ($\phi_{oil} = 1.0$), we observed $\tau_{ice} \gg 0$. In all of our

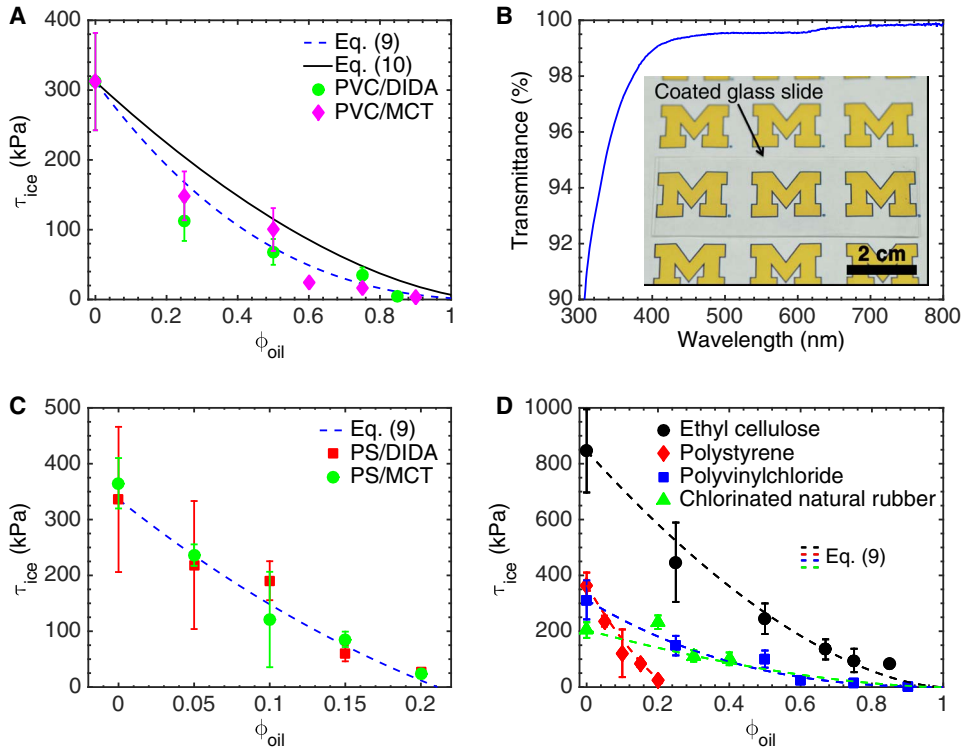

Fig. 4. Icephobic linear polymers. (**A**) PVC plasticized with MCT oil or DIDA showed a good agreement with Eq. 9 and excellent icephobicity after $\phi_{oil} > 0.5$. (**B**) All the icephobic, linear polymers discussed in this work were >98% transparent. Here, we show the transmittance versus wavelength for PVC plasticized with 50 wt % MCT oil. The inset shows an optical image of the same coating. (**C**) PS became icephobic at very low concentrations of plasticizer but still fit the proposed theory extremely well. (**D**) An excellent agreement was observed between Eq. 9 and the ice adhesion strength values for the four different polymers plasticized with MCT oil.

other systems, we have never observed values of ϕ_{oil} in the red region of our icephobicity phase diagram.

If $\phi_{oil} > \phi_{oil}^{max}$, then the polymer's oil capacity has been exceeded, and the surface is necessarily lubricated. Any lubricated system should exhibit an ice adhesion strength less than

$$\frac{\tau_{ice}^{oil}}{\tau_{ice}^{no-oil}} = \left(1 - \phi_{oil}^{max}\right)^{5/3}(1 - \alpha) \quad (11)$$

This lower bound separates the interfacial slippage regime (green region) from the lubrication regime (blue region) in our phase diagram (Fig. 5A). However, recall that the ice adhesion strength of lubricated surfaces increases over time (*7*, *10*), making Eq. 11 a predictor for the ice adhesion strength that lubricated polymers will exhibit once their lubricating layer has been removed. Lubricated polymers may therefore prove advantageous over lubricant-infused surfaces (*8*, *32*). Lubricant-infused surfaces are based on textured solids for which $\phi_{oil}^{max} \approx 0$, and therefore, τ_{ice}^{no-oil} is very high (*33*, *34*). To illustrate this point, we fabricated lubricated rubbers by overfilling ($\phi_{oil} \gg \phi_{oil}^{max}$) the VF40 rubber with four oils of varying miscibility [ϕ_{oil}^{max} = 0.07, 0.17, 0.29, or 0.51, for squalane oil, high-oleic SFO (HO SFO), HL SFO, and MCT oil, respectively]. All the initial τ_{ice} values fell within the predicted lubrication regime (open symbols, Fig. 5B). Upon wiping the free oil layer from the surface of the lubricated rubber, simulating a complete loss of lubricant, we observed an exceptional agreement with Eq. 11 and the subsequently measured τ_{ice} values of these four elastomer/oil combinations (closed symbols, Fig. 5B).

The ice adhesion strength of polymeric systems will always be bounded by Eq. 10 (plasticizer completely in the bulk) and Eq. 11 (maximum amount of miscible plasticizer on the surface). A good agreement was found between these two limiting equations and the 11 different systems presented in this study (Fig. 5C and Materials and Methods). The ice adhesion strengths for 10 different icephobic formulations—ranging in base material, ϕ_{oil}, and fabrication technique (Materials and Methods)—are presented in Table 1.

As an example highlighting the usefulness of Fig. 5A, consider some extremely durable polymer with τ_{ice} = 300 kPa. This material is not icephobic. For some applications, $\tau_{ice} \leq 30$ kPa is necessary (*6*, *7*, *33*). What oil, and how much oil, should be incorporated for the icephobic coating to achieve this desired ice adhesion strength? According to Fig. 5A, a reduction in the ice adhesion strength ratio to 0.1 necessitates that the coating is at least 47% oil. Any less than 47% oil within the coating will not result in the required ice adhesion strength unless the surface is fully lubricated. No more than 75% oil is necessary, because Eq. 10 dictates that an even lower ice adhesion strength will be achieved for $\phi_{oil} \geq 0.75$. Thus, an oil must be selected where $\phi_{oil}^{max} > 0.47$, and the amount of oil added should be $0.47 \leq \phi_{oil} \leq 0.75$. Should this material instead be lubricated, for example, with an oil for which $\phi_{oil}^{max} = 0.2$, the ice adhesion strength will increase to $\tau_{ice} \approx 60$ kPa once the oil is depleted, and the coating will become ineffective. PVC, a durable engineering plastic, displayed a nonplasticized ice adhesion strength of $\tau_{ice}^{no-oil} = 312 \pm 70$ kPa. When plasticized with 60 wt % MCT oil, for which $\phi_{oil}^{max} \approx 0.9$, the ice adhesion strength reduced to $\tau_{ice} = 24 \pm 4$ kPa and did not increase over 10 icing/deicing cycles. In contrast, CF50, a polyurethane ($\tau_{ice}^{no-oil} = 319 \pm 44$ kPa), lubricated with MCT oil (for which $\phi_{oil}^{max} \approx 0.07$)

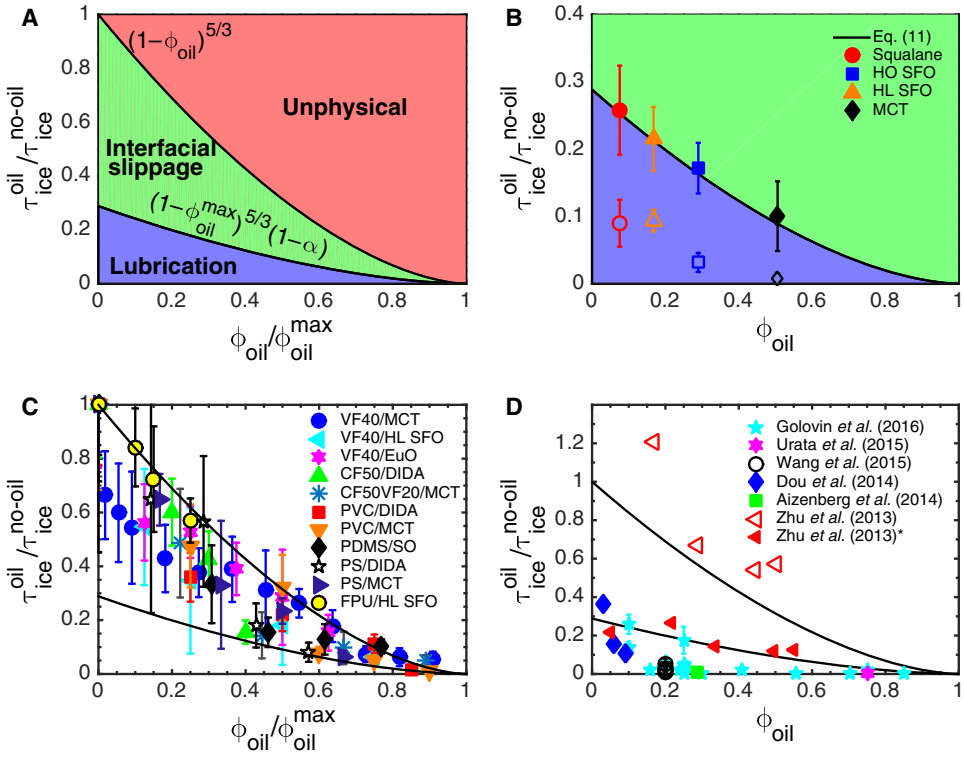

Fig. 5. Designing icephobic surfaces. (**A**) Phase diagram for icephobic polymers. The regime of possible durability, the green region containing surfaces using interfacial slippage, is bounded by Eqs. 10 and 11. (**B**) When VF40 was lubricated with four oils of differing solubility, the initial τ_{ice} values (open symbols) fell within the lubrication regime. Equation 11 precisely predicted the reduction in the values for the ice adhesion strength upon wiping away the free oil layer (closed symbols). (**C**) For 11 different polymer/plasticizer combinations, our measured reductions in τ_{ice} for surfaces that exhibited interfacial slippage were always bounded by Eqs. 10 and 11. Note that, for the FPU/HL SFO system, the solid surface energy was lower than the surface tension of the plasticizer. (**D**) Lubricated elastomers from previous studies can initially achieve ultralow reductions in τ_{ice}, and the reported τ_{ice} values correctly lay in the lubrication region predicted by Eq. 11. The data from Zhu *et al.* (*11*), recast using the literature τ_{ice} value for PDMS, is denoted by an asterisk. For the data of Wang *et al.* (*10*), only one ϕ_{oil} value was reported, so all the surfaces have been placed at this value.

initially displayed $\tau_{ice} \approx 14$ kPa. When the MCT oil was wiped away, the observed ice adhesion strength increased to $\tau_{ice} \approx 150$ kPa.

The above examples illustrate why engineering icephobic surfaces that display $\tau_{ice} \leq 30$ kPa without lubrication has been challenging in the past. Almost all materials exhibit $\tau_{ice}^{no-oil} > 200$ kPa (*12*), making the precise choice of oil and oil content necessary. The above examples also illustrate why several lubricated, icephobic systems have been reported (*4*–*6*, *8*–*11*), whereas we have only recently observed ultralow ice adhesion strengths without the use of lubrication (*7*). In Fig. 5D, we compile six previous studies on lubricated, icephobic rubbers. Almost all the τ_{ice} values for these lubricated systems fall into the region of lubrication predicted by our phase diagram. Once the lubricants are removed, the ice adhesion strengths should increase to values given by Eq. 11. Note that the τ_{ice} values for the surfaces created by Zhu *et al.*(*11*) fall outside the allowable range predicted by our framework, although the surface was a mixture of PDMS and silicone oil, similar to surfaces in this work (Fig. 3C) and in the studies of Urata *et al.* (*9*) and Aizenberg *et al.* (*4*). The ice adhesion of the unfilled PDMS in the work of Zhu *et al.* was reported to be $\tau_{ice} = 55$ kPa, much lower than the accepted literature value of $\tau_{ice} =$ 250 to 300 kPa (*7*, *12*, *22*). It is likely that unreacted siloxane chains enabled interfacial slippage in their unfilled PDMS, a previously reported phenomenon (*7*, *30*). Recasting their data using the literature value for the ice adhesion strength of PDMS placed their measured τ_{ice} values correctly near the lubrication regime.

CONCLUSIONS

Here, we have built a framework that predicts the reduction in the ice adhesion strength of both thermoplastics and thermosets, based on the addition of an oil/plasticizer. The addition of a plasticizer lowers the ice adhesion in two ways: by lowering the effective cross-link density or modulus of the polymer and by making only a fraction of the polymer's surface available to adhere to ice. An excellent agreement was observed between our framework, Eq. 9, and a wide range of polymer/plasticizer combinations. Moreover, the use of Eq. 11 allows lubricated systems to be fabricated with full knowledge of their expected ice adhesion strength once the lubricant becomes depleted. Overall, our proposed framework will allow for a wide range of icephobic materials to be fabricated from essentially any chemistry and base components. Many of the formulations exemplified in this work may find immediate usage for solving the ice accretion problem in a host of different sectors worldwide.

MATERIALS AND METHODS

Sample fabrication

VF40, VF20, and CF50 (Smooth-On Inc.) or Sylgard 184 (Dow Corning) were mixed per manufacturer's instructions. PB-6 (Soltex Solvents), MCT oil, eucalyptus oil, jojoba oil, HL SFO, HO SFO, and squalane oil (Jedwards International), or DIDA, DUP, 100-cP silicone oil, and *n*-hexadecane (Sigma-Aldrich) were added to the liquid prepolymer,

and the solution was vortexed until it was homogeneous. The mixtures were then poured onto glass slides and allowed to cure at room temperature (VF) or at 80°C (CF and PDMS) overnight. For the CF50VF20 coating in Table 1, equal parts of the two polymers were combined.

PVC (M_w = 120,000 g/mol, Scientific Polymer) was dissolved in a 60/40 (v/v) mixture of acetone and *n*-methyl pyrrolidone (Sigma-Aldrich). First, a stock solution at a concentration of 100 mg/ml of PVC in this solvent mixture was formed. Once fully dissolved, MCT or DIDA was added to the solution, and the system was homogenized using a vortexer at room temperature. The solution was poured onto glass slides, and the solvent was allowed to evaporate on a 40°C hotplate overnight. PS (M_w = 190,000 g/mol; Scientific Polymer) or chlorinated natural rubber (Pergut S 10, Covestro) was dissolved in toluene (Sigma-Aldrich) at a concentration of 500 mg/ml. Either MCT or DIDA was added, and the solution was homogenized using a vortexer. The solution was poured onto glass slides, and the toluene was allowed to evaporate on a 50°C hotplate overnight. Ethyl cellulose (Scientific Polymer #142) was dissolved in toluene at a concentration of 100 mg/ml. MCT was added, and the solution was homogenized using a vortexer. The solution was poured onto glass slides, and the toluene was allowed to evaporate on a 50°C hotplate overnight.

Swelling and ice adhesion testing

Cross-link densities were measured by swelling 50- to 200-mg pieces of the various oil-filled elastomers in excess toluene. After 24 hours, the toluene was exchanged to remove any oil extracted from the swollen rubber samples. The weight was recorded daily. Once a constant mass was achieved, the samples were placed in a 120°C oven under vacuum to remove the toluene. The final mass was recorded after the toluene was completely removed. The swell ratio was defined as the ratio of the swollen mass to the final mass, after the solvent and oil were completely extracted. To determine the maximum solubility of an oil in a cross-linked network, we placed pieces of the polymer in vials of excess oil. A similar procedure as above was followed. Note that the higher molecular weight of the oils used in this work necessitated large diffusion times before equilibrium swelling was achieved (up to 8 weeks in some cases).

The ice adhesion strength was measured using a custom setup described previously (*7*). Briefly, a force gauge was mounted to a movable stage. The gauge pushed the ice adhered to a substrate atop a Peltier plate. The thickness of the ice was ≈5 to 8 mm, whereas the gauge contacted the surface <1 mm from the surface. Testing was done at −10°C. Water (500 μl) was used for all measurements. Surfaces are allowed sufficient time to fully freeze before testing. A Mark-10 force gauge with a minimum resolution of 0.0005 N was used to measure τ_{ice} for surfaces with $\tau_{ice} \leq 100$ kPa. An Imada force gauge was used for surfaces with $\tau_{ice} > 100$ kPa, which has a resolution of 0.1 N. The reported τ_{ice} values are the average of at least six independent measurements.

Surface fraction determination

The fraction of oil on the surface of the oil-filled polymers was determined through the method of hemi-wicking using a Ramé-Hart 200-F1 goniometer. A ≈10-μl drop of oil was advanced on the surface of the polymer plasticized with the same oil. The advancing contact angle was used in place of θ. Use of the advancing contact angle largely avoided any temporal effects (for example, swelling of the elastomer during contact angle measurement). For every elastomer/oil combination evaluated, the receding contact angle was always 0°. The values used to determine ϕ_s were the average of at least five measurements, and the typical error in the measurements was ±2°. Note that samples containing $\phi_{oil} > \phi_{oil}^{max}$ were necessary to achieve $\phi_s \approx 0$. This occurred partly because we chose to use the advancing contact angle for our measurements and partly because, at $\phi_{oil} = \phi_{oil}^{max}$, additional oil was required to form a thick film on the surface of the elastomer. However, this matched well with our assumption that $\tau_{ice} = 0$ when $\phi_s = 0$, that is, for surfaces fabricated with $\phi_{oil} = \phi_{oil}^{max}$, we always observed $\tau_{ice} > 0$ (although typically $\tau_{ice} < 5$ kPa).

Transparency analysis

Optical transparency of the PVC sample was measured using a Varian Cary 50 Bio UV-Vis spectrometer. A scan range of 200 to 800 nm was probed using a scan rate of 600 nm/s. Glass was used as a baseline.

SUPPLEMENTARY MATERIALS

Supplementary material for this article is available at http://advances.sciencemag.org/cgi/content/full/3/9/e1701617/DC1

Supplementary Text

table S1. ϕ_{oil}^{max} for four elastomers and 10 different oils.

table S2. Ice adhesion data for each plasticized polymer considered in this work.

fig. S1. Durability of highly plasticized PVC.

REFERENCES AND NOTES

1. N. D. Mulherin, R. B. Haehnel, *Ice Engineering: Progress in Evaluating Surface Coatings for Icing Control at Corps Hydraulic Structures* (U.S. Army Engineer Research and Development Center, 2003).
2. J. Shin, T. H. Bond, Surface roughness due to residual ice in the use of low power deicing systems, paper presented at the 31st Aerospace Sciences Meeting and Exhibit, Reno, NV, 01 January 1993.
3. V. Hejazi, K. Sobolev, M. Nosonovsky, From superhydrophobicity to icephobicity: Forces and interaction analysis. *Sci. Rep.* **3**, 2194 (2013).
4. J. Aizenberg, M. Aizenberg, J. Cui, B. Hatton, S. Dunn, C. Howell, P. Kim, T. S. Wong, U.S. Patent WO2014012080A1 (2014).
5. J. Chen, R. Dou, D. Cui, Q. Zhang, Y. Zhang, F. Xu, X. Zhou, J. Wang, Y. Song, L. Jiang, Robust prototypical anti-icing coatings with a self-lubricating liquid water layer between ice and substrate. *ACS Appl. Mater. Interfaces* **5**, 4026–4030 (2013).
6. R. Dou, J. Chen, Y. Zhang, X. Wang, D. Cui, Y. Song, L. Jiang, J. Wang, Anti-icing coating with an aqueous lubricating layer. *ACS Appl. Mater. Interfaces* **6**, 6998–7003 (2014).
7. K. Golovin, S. P. R. Kobaku, D. H. Lee, E. T. DiLoreto, J. M. Mabry, A. Tuteja, Designing durable icephobic surfaces. *Sci. Adv.* **2**, e1501496 (2016).
8. P. Kim, T.-S. Wong, J. Alvarenga, M. J. Kreder, W. E. Adorno-Martinez, J. Aizenberg, Liquid-infused nanostructured surfaces with extreme anti-ice and anti-frost performance. *ACS Nano* **6**, 6569–6577 (2012).
9. C. Urata, G. J. Dunderdale, M. W. England, A. Hozumi, Self-lubricating organogels (SLUGs) with exceptional syneresis-induced anti-sticking properties against viscous emulsions and ices. *J. Mater. Chem. A* **3**, 12626–12630 (2015).
10. Y. Wang, X. Yao, J. Chen, Z. He, J. Liu, Q. Li, J. Wang, L. Jiang, Organogel as durable anti-icing coatings. *Sci. China Mater.* **58**, 559–565 (2015).
11. L. Zhu, J. Xue, Y. Wang, Q. Chen, J. Ding, Q. Wang, Ice-phobic coatings based on silicon-oil-infused polydimethylsiloxane. *ACS Appl. Mater. Interfaces* **5**, 4053–4062 (2013).
12. A. J. Meuler, J. D. Smith, K. K. Varanasi, J. M. Mabry, G. H. McKinley, R. E. Cohen, Relationships between water wettability and ice adhesion. *ACS Appl. Mater. Interfaces* **2**, 3100–3110 (2010).
13. H. Murase, K. Nanishi, On the relationship of thermodynamic and physical properties of polymers with ice adhesion. *Ann. Glaciol.* **6**, 146–149 (1985).
14. O. Parent, A. Ilinca, Anti-icing and de-icing techniques for wind turbines: Critical review. *Cold Reg. Sci. Technol.* **65**, 88–96 (2011).
15. T. Burton, N. Jenkins, D. Sharpe, E. Bossanyi, *Wind Energy Handbook* (John Wiley & Sons Ltd., 2011).
16. M. K. Chaudhury, K. H. Kim, Shear-induced adhesive failure of a rigid slab in contact with a thin confined film. *Eur. Phys. J. E Soft Matter* **23**, 175–183 (2007).
17. J. P. Rothstein, Slip on superhydrophobic surfaces. *Annu. Rev. Fluid Mech.* **42**, 89–109 (2010).
18. K. B. Migler, H. Hervet, L. Leger, Slip transition of a polymer melt under shear stress. *Phys. Rev. Lett.* **70**, 287–290 (1993).

19. Y. B. Chernyak, A. I. Leonov, On the theory of the adhesive friction of elastomers. *Wear* **108**, 105–138 (1986).
20. C. L. M. H. Navier, Mémoire sur les lois du mouvement des fluides. *Mém. Acad. Sci. Inst. France* **6**, 389–440 (1823).
21. D. L. Beemer, W. Wang, A. K. Kota, Durable gels with ultra-low adhesion to ice. *J. Mater. Chem. A* **4**, 18253–18258 (2016).
22. C. Wang, T. Fuller, W. Zhang, K. J. Wynne, Thickness dependence of ice removal stress for a polydimethylsiloxane nanocomposite: Sylgard 184. *Langmuir* **30**, 12819–12826 (2014).
23. G. Wypych, *Handbook of Plasticizers* (ChemTec Publishing, ed. 2, 2012).
24. P. J. Flory, J. Rehner Jr., Statistical theory of chain configuration and physical properties of high polymers. *Ann. N. Y. Acad. Sci.* **44**, 419–429 (1943).
25. P.-G. de Gennes, F. Brochard-Wyart, D. Quere, *Capillarity and Wetting Phenomena: Drops, Bubbles, Pearls, Waves* (Springer, 2004).
26. J. Bico, U. Thiele, D. Que´re´, Wetting of textured surfaces. *Colloids Surf. A* **206**, 41–46 (2002).
27. G. Kraus, Swelling of filler-reinforced vulcanizates. *J. Appl. Polym. Sci.* **7**, 861–871 (1963).
28. J. Krawczyk, S. Croce, T. C. B. McLeish, B. Chakrabarti, Elasticity dominated surface segregation of small molecules in polymer mixtures. *Phys. Rev. Lett.* **116**, 208301 (2016).
29. C. M. Hansen, *Hansen Solubility Parameters: A User's Handbook* (CRC Press, ed. 2, 2007).
30. J. N. Lee, C. Park, G. M. Whitesides, Solvent compatibility of poly(dimethylsiloxane)-based microfluidic devices. *Anal. Chem.* **75**, 6544–6554 (2003).
31. J. E. Mark, *Polymer Data Handbook* (Oxford Univ. Press, ed. 2, 2009).
32. S. B. Subramanyam, K. Rykaczewski, K. K. Varanasi, Ice adhesion on lubricant-impregnated textured surfaces. *Langmuir* **29**, 13414–13418 (2013).
33. M. J. Kreder, J. Alvarenga, P. Kim, J. Aizenberg, Design of anti-icing surfaces: Smooth, textured or slippery? *Nat. Rev. Mater.* **1**, 15003 (2016).
34. K. K. Varanasi, T. Deng, J. D. Smith, M. Hsu, N. Bhate, Frost formation and ice adhesion on superhydrophobic surfaces. *Appl. Phys. Lett.* **97**, 234102 (2010).

Acknowledgments

Funding: We thank K.-H. Kim and the Office of Naval Research for the financial support under grant N00014-12-1-0874. We also thank C. Y. Lee and the Air Force Office of Scientific Research for the financial support under grants FA9550-15-1-0329. We also thank the NSF and the Nanomanufacturing Program for supporting this work through grant #1351412. K.G. thanks the Department of Defense for a National Defense Science and Engineering Graduate Fellowship. **Author contributions:** K.G. conceived the research, designed, and performed all experiments and wrote the manuscript. A.T. conceived the research, designed the experiments, and wrote the manuscript. **Competing interests:** A.T. and K.G. are authors on a patent application related to this work filed by the University of Michigan (application no. 62/153,141, filed 27 April 2015). A.T. is the chief technology officer of and has been a paid consultant for HygraTek LLC. K.G. is a current employee of HygraTek LLC. The authors declare that they have no other competing interests. **Data and materials availability:** All data needed to evaluate the conclusions in the paper are present in the paper and/or the Supplementary Materials. Additional data related to this paper may be requested from the authors.

Submitted 15 May 2017
Accepted 28 August 2017
Published 22 September 2017
10.1126/sciadv.1701617

Citation: K. Golovin, A. Tuteja, A predictive framework for the design and fabrication of icephobic polymers. *Sci. Adv.* **3**, e1701617 (2017).

A predictive framework for the design and fabrication of icephobic polymers

Kevin Golovin and Anish Tuteja

Sci Adv **3** (9), e1701617.
DOI: 10.1126/sciadv.1701617